

Mode-sum renormalization of $\langle\Phi^2\rangle$ for a quantum scalar field inside a Schwarzschild black hole

Assaf Lanir, Adam Levi and Amos Ori

Department of physics, Technion-Israel Institute of Technology, Haifa 32000, Israel

The full computation of the renormalized expectation values $\langle\Phi^2\rangle_{ren}$ and $\langle\hat{T}_{\mu\nu}\rangle_{ren}$ in 4D black hole interiors has been a long standing challenge, which has impeded the investigation of quantum effects on the internal structure of black holes for decades. Employing a recently developed mode sum renormalization scheme to numerically implement the point-splitting method, we report here the first computation of $\langle\Phi^2\rangle_{ren}$ in Unruh state in the region inside the event horizon of a 4D Schwarzschild black hole. We further present its Hartle-Hawking counterpart, which we calculated using the same method, and obtain a fairly good agreement with previous results attained using an entirely different method by Candelas and Jensen in 1986. Our results further agree upon approaching the event horizon when compared with previous results calculated outside the black hole. Finally, the results we obtained for Hartle-Hawking state at the event horizon agree with previous analytical results published by Candelas in 1980. This work sets the stage for further explorations of $\langle\Phi^2\rangle_{ren}$ and $\langle\hat{T}_{\mu\nu}\rangle_{ren}$ in 4D black hole interiors.

I. INTRODUCTION

It is well known that classical matter fields on black hole (BH) backgrounds can considerably modify the interior geometry. Consider, for instance, the unperturbed Reissner-Nordström (RN) and Kerr solutions. Both solutions possess an inner horizon, which is a perfectly regular null hypersurface. However, classical perturbations, both linear and nonlinear, were shown to result in the formation of a weak null curvature singularity along the ingoing section of the inner horizon, in four dimensional spinning [1–5] and spherically-symmetric charged BHs [6–10]. A different example for the modification that classical perturbations impose upon BH interior geometry is the effective shock wave singularity developing along the outgoing section of the inner horizon [11–13]. It is therefore reasonable to expect that quantum matter fields would also affect the BH interior geometry. Indeed, semiclassical general relativity, in its turn, proved to have the potential to drastically influence the evolution of BHs. It implies, for example, that BHs emit radiation and evaporate, as was shown in an analysis by Hawking [14]. This process results in a spacetime structure radically different from the classical BH structure. It therefore seems conceivable that semiclassical stress-energy fluxes could potentially affect the inner horizon of the RN and Kerr solutions in a different manner than the classical perturbations considered thus far. In particular, one may consider the scenario where semiclassical effects convert the classical weak null singularity into a strong (i.e. tidally destructive) spacelike one. Or alternatively, one may entertain the thought that semiclassical effects might actually resolve the strong spacelike singularity in Schwarzschild spacetime. These are profound issues that remain as yet unresolved.

Interested as we are in the internal structure of BHs, we must therefore investigate the semiclassical picture of BH interiors. Semiclassical gravity considers quantum field theory in curved spacetime, where gravitation is treated classically, i.e. describing spacetime structure as a Lorentzian manifold that is equipped with a metric $g_{\mu\nu}$. At the same time, the matter fields propagating in that classical background are quantum fields. The relation between spacetime geometry and the stress-energy of the quantum matter fields is described by the semiclassical Einstein's field equation

$$G_{\mu\nu} = 8\pi\langle\hat{T}_{\mu\nu}\rangle_{ren}. \quad (1.1)$$

Here $G_{\mu\nu}$ is the Einstein tensor of spacetime, and $\langle\hat{T}_{\mu\nu}\rangle_{ren}$ is the *renormalized stress-energy tensor* (RSET), which is the renormalized expectation value of the stress-energy tensor operator $\hat{T}_{\mu\nu}$, associated with the quantum fields. In Eq. (1.1) and throughout this paper we adopt standard geometric units $c = G = 1$, along with the metric signature $(-+++)$.

As already mentioned, we are generally interested in the internal structure of BHs within the semiclassical framework, and especially in the effect of quantum fields on the inner horizons of RN and Kerr BHs. To this end, we have initiated a research program aimed to compute the RSET on BH backgrounds. In the present work we focus attention on the interior of a Schwarzschild BH, which is interesting in its own right. As an example of a quantum field we take

for simplicity a massless scalar field, satisfying the massless Klein-Gordon equation¹

$$\square_g \hat{\Phi} = 0, \quad (1.2)$$

where $\hat{\Phi}$ is the scalar field operator, and the covariant D'Alembertian operator is used with respect to the background spacetime metric, denoted by g , the Schwarzschild metric in the present case. Although the physically more interesting object is the RSET, it is useful to first compute $\langle \Phi^2 \rangle_{ren}$ as it is technically simpler, yet it still captures many of the RSET's essential features, thereby serving as a simple toy-model for it.

However, the computation of $\langle \Phi^2 \rangle_{ren}$ (and of other composite operators, including the RSET) in a general curved spacetime is a tremendously difficult task. The naive computation yields a divergent series of modes which requires renormalization. A renormalization method based on point-splitting was developed by Christensen [15, 16]. He employed the DeWitt-Schwinger expansion of Feynman's Green function [17, 18] (see also [19]) in order to compute $\langle \Phi^2 \rangle_{ren}$ (and similarly the RSET, $\langle \hat{T}_{\mu\nu} \rangle_{ren}$). The basic idea is to regularize the expectation value by splitting the point x , at which $\langle \Phi^2(x) \rangle_{ren}$ is to be evaluated, into a separated pair of points x and x' , and consider the two-point function $\langle \hat{\Phi}(x) \hat{\Phi}(x') \rangle$. It is convenient and common - and we shall be adhering to that convention - to consider, instead of the two-point function, the Hadamard function which is related in a simple way to the two-point function and is defined as

$$G^{(1)}(x, x') = \langle \{ \hat{\Phi}(x), \hat{\Phi}(x') \} \rangle, \quad (1.3)$$

where $\{, \}$ denotes anti-commutation. A specific counter-term, which is a local geometric object depending on the background metric and independent of the quantum state, is then subtracted from the Hadamard function. Finally the limit $x' \rightarrow x$ is taken, yielding $\langle \Phi^2 \rangle_{ren}$. A similar procedure can be applied to the computation of the RSET and of other composite operators which are quadratic in the field operator and its derivatives.

This point-splitting scheme works fine in situations where the scalar field modes can be analytically computed. Unfortunately, in BH backgrounds the modes must be numerically computed, and as a result the procedure by Christensen, as is, is impractical. Nevertheless, practical methods that numerically implement the point-splitting scheme were later developed by Candelas, Howard, Anderson and others [16, 20–23], allowing for the computation of $\langle \Phi^2 \rangle_{ren}$ and the RSET, usually requiring a high-order WKB expansion for the field modes. Seeing as this is highly difficult to carry out in the Lorentzian section of spacetime, a Wick rotation to the Euclidean section is usually performed. This approach restricts the background spacetimes where the renormalization procedure can be applied, since a generic spacetime does not admit a Euclidean section.

The *pragmatic mode-sum regularization* (PMR) scheme, recently developed by two of the authors (AL and AO), offers a more versatile method to numerically implement the point-splitting scheme. It relies neither on a Euclidean section nor on a WKB expansion. It only requires a single Killing field in the background spacetime. The PMR method was used [24–28] to compute $\langle \Phi^2 \rangle_{ren}$ and the RSET outside the event horizons of the three canonical BH solutions, namely Schwarzschild, RN (unpublished), and Kerr.

So far, most of the calculations of $\langle \Phi^2 \rangle_{ren}$ and the RSET were carried out in the regions exterior to the event horizon of BHs. We are only aware of a single exception presented in Ref. [29], where $\langle \Phi^2 \rangle_{ren}$ was calculated in the interior region of a Schwarzschild BH, in the Hartle-Hawking state [30, 31]. A possible reason for that may be that the computation in BH interiors entails intricate analytic derivations, expressing the Hadamard function by the standard Eddington-Finkelstein modes, and it further involves tedious numerical computations in both regions, interior and exterior. The present work implements the angular-splitting (or “ θ -splitting”) variant of the PMR method, introduced in [25], to compute $\langle \Phi^2 \rangle_{ren}$ in the interior region of a Schwarzschild BH, as a first stage before computing it in the interior of RN. We employed the PMR method in the Hartle-Hawking state to recover the results appearing in [29] in the domain $M \leq r < 2M$, and we found a fairly good agreement. We further compute $\langle \Phi^2 \rangle_{ren}$ in the Unruh state [32] (in the same range of r), which is physically more interesting as it describes an evaporating BH. Our results for $\langle \Phi^2 \rangle_{ren}$ in both quantum states (i.e. Hartle-Hawking and Unruh) show nice agreement with previous analogous results obtained outside the BH [25] when compared at the event horizon, where both sets of results meet.

The organization of this paper is as follows. In section II we introduce necessary preliminaries needed for the computation of $\langle \Phi^2 \rangle_{ren}$. Then, in section III we briefly present the key steps in the renormalization procedure we use in the computation. Section IV presents the details of the numerical implementation and the results we obtained for $\langle \Phi^2 \rangle_{ren}$. In section V we discuss our results and possible extensions.

¹ The Klein-Gordon equation for a nonminimally-coupled massless scalar field also includes the term $\xi R \hat{\Phi}$, where R is the Ricci scalar. However, we are considering here a Schwarzschild spacetime where the Ricci scalar vanishes.

II. PRELIMINARIES

Before we delve into the details of the numerical implementation of the angular-splitting variant of the PMR method inside the Schwarzschild event horizon, let us precede by establishing the basic definitions of coordinate systems, sets of modes, and quantum states which we use in the present work. We also write down the form of the Hadamard function inside the event horizon of a Schwarzschild BH, for both Hartle-Hawking and Unruh states. This preliminary section summarizes the relevant definitions and results of [33], with the reservation that Ref. [33] considers RN BHs. Specializing to the Schwarzschild case simply amounts to taking the limit where the electric charge of the BH vanishes.

A. Coordinate systems

The line element of the Schwarzschild solution in the standard Schwarzschild coordinates takes the form

$$ds^2 = -f dt^2 + f^{-1} dr^2 + r^2 (d\theta^2 + \sin^2 \theta d\varphi^2), \quad (2.1)$$

where

$$f = 1 - \frac{2M}{r}. \quad (2.2)$$

The event horizon, $r = r_s$, is located at the root of f , i.e.

$$r_s = 2M.$$

The surface gravity parameter, κ , is given by

$$\kappa = \frac{1}{4M}.$$

We define the tortoise coordinate, r_* , in both the interior and the exterior regions, using the standard relation

$$\frac{dr}{dr_*} = 1 - \frac{2M}{r}.$$

Specifically, we choose the integration constants in the interior and the exterior regions such that in both regions

$$r_* = r + 2M \ln \left(\left| 1 - \frac{r}{2M} \right| \right).$$

Note that r_s corresponds to $r_* \rightarrow -\infty$ (both inside and outside the BH), and $r = 0$ to $r_* \rightarrow 0$.

The Eddington-Finkelstein coordinates are defined in the exterior and interior regions by

$$u_{\text{ext}} = t - r_* \quad , \quad v = t + r_*, \quad (\text{outside})$$

and

$$u_{\text{int}} = r_* - t \quad , \quad v = r_* + t, \quad (\text{inside}).$$

Note that the v coordinate is continuously defined throughout both regions I and II of Fig. 1.

The Kruskal coordinates are defined in terms of the exterior and interior Eddington-Finkelstein coordinates by

$$U(u_{\text{ext}}) = -\frac{1}{\kappa} \exp(-\kappa u_{\text{ext}}) \quad , \quad V(v) = \frac{1}{\kappa} \exp(\kappa v), \quad (\text{outside}) \quad (2.3)$$

and

$$U(u_{\text{int}}) = \frac{1}{\kappa} \exp(\kappa u_{\text{int}}) \quad , \quad V(v) = \frac{1}{\kappa} \exp(\kappa v), \quad (\text{inside}). \quad (2.4)$$

We make the following notations: H_{past} denotes the past horizon [i.e. the hypersurface ($U < 0, V = 0$)], and PNI denotes past null infinity [i.e. ($U = -\infty, V > 0$)]. H_L is the ‘‘left event horizon’’ ($U > 0, V = 0$), and H_R is the ‘‘right event horizon’’ ($U = 0, V > 0$). See Fig. 1.

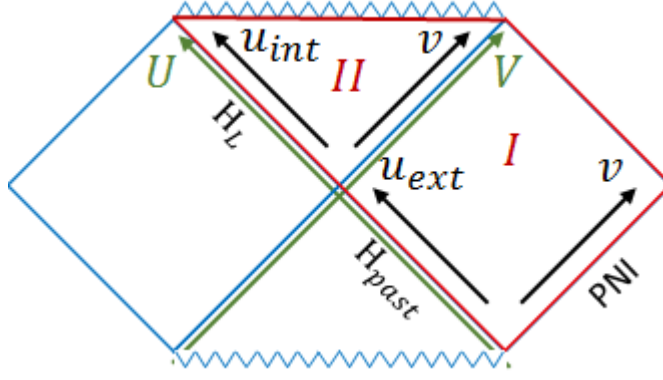


Figure 1: Penrose diagram of Schwarzschild spacetime. In the exterior region (region I), we use the external Eddington-Finkelstein coordinates, while in the interior (region II), we use the internal ones. In addition, the Kruskal coordinate system is shown in green and is defined throughout both regions I and II . The red-framed area denotes the region in the eternal Schwarzschild spacetime which concerns this paper, i.e. regions I and II .

B. Sets of modes and quantum states

Recall that the matter field we are considering here is a massless quantum scalar field satisfying the D'Alembertian equation (1.2) on Schwarzschild background. This field can be decomposed into sets of modes satisfying Eq. (1.2). By choosing certain sets of modes, one can define several quantum states of interest. To this end, it will be useful to consider various complete sets of modes outside and inside the event horizon.

Let us begin with the definition of the *Unruh modes* for positive ω , which we denote by $g_{\omega lm}^{\text{up}}$ and $g_{\omega lm}^{\text{in}}$. We first use the spherical symmetry to decompose the modes in the following standard way:

$$g_{\omega lm}^{\Lambda}(x) = \omega^{-1/2} C_{lm}(x) \tilde{g}_{\omega l}^{\Lambda}(x), \quad (2.5)$$

where

$$C_{lm}(x) = (4\pi)^{-1/2} \frac{1}{r} Y_{lm}(\theta, \varphi). \quad (2.6)$$

Here the index Λ denotes “in” and “up”, and the factor $1/\sqrt{4\pi\omega}$ was introduced to ensure proper normalization under the Klein-Gordon inner product. Furthermore, $\tilde{g}_{\omega l}^{\Lambda}$ are solutions of the following two-dimensional wave equation, obtained by substituting Eq. (2.5) in Eq. (1.2):

$$\tilde{g}_{,r^*r^*}^{\Lambda} - \tilde{g}_{,tt}^{\Lambda} = V_l(r) \tilde{g}^{\Lambda}, \quad (2.7)$$

where

$$V_l(r) = \left(1 - \frac{2M}{r}\right) \left[\frac{l(l+1)}{r^2} + \frac{2M}{r^3}\right]. \quad (2.8)$$

The Unruh modes are then defined by requiring the two sets of independent solutions, $\tilde{g}_{\omega l}^{\text{up}}$ and $\tilde{g}_{\omega l}^{\text{in}}$, to satisfy the following initial conditions:

$$\tilde{g}_{\omega l}^{\text{up}} = \begin{cases} e^{-i\omega U} & , & H_{\text{past}} \\ e^{-i\omega U} & , & H_L \\ 0 & , & \text{PNI} \end{cases}, \quad \tilde{g}_{\omega l}^{\text{in}} = \begin{cases} 0 & , & H_{\text{past}} \\ 0 & , & H_L \\ e^{-i\omega v} & , & \text{PNI} \end{cases}. \quad (2.9)$$

Note that the Unruh modes are defined both inside and outside the event horizon, i.e. they are defined throughout the red-framed regions I and II in Fig. 1.

Using these modes, the quantum scalar field operator is decomposed as follows:

$$\hat{\Phi}(x) = \int_0^{\infty} d\omega \sum_{\Lambda, l, m} \left[g_{\omega lm}^{\Lambda}(x) \hat{a}_{\omega lm}^{\Lambda} + g_{\omega lm}^{\Lambda*}(x) \hat{a}_{\omega lm}^{\Lambda\dagger} \right], \quad (2.10)$$

and the Unruh state, $|0\rangle_U$, is defined as the quantum state annihilated by the operators $\hat{a}_{\omega lm}^\Lambda$ appearing in (2.10), i.e.

$$\hat{a}_{\omega lm}^\Lambda |0\rangle_U = 0$$

(for all Λ and ωlm). As was mentioned in the introduction, the Unruh state is physically interesting, as it describes an evaporation of a BH [32]. The vacuum expectation value of the stress-energy tensor in this state is regular at the event horizon (H_R), but not at the past horizon (H_{past}) [34].

Let us now proceed to the definition of the *outer Eddington-Finkelstein modes*, $f_{\omega lm}^{\text{up}}$ and $f_{\omega lm}^{\text{in}}$, for positive ω (these are also known as the *Boulware modes*, as they are closely related to the Boulware state [35]). Again, we decompose the modes like we did in Eq. (2.5) above:

$$f_{\omega lm}^\Lambda(x) = |\omega|^{-1/2} C_{lm}(x) \tilde{f}_{\omega l}^\Lambda(x), \quad (2.11)$$

where C_{lm} is the same function appearing in Eq. (2.6) and the index Λ again stands for “in” and “up”. The functions $\tilde{f}_{\omega l}^\Lambda$, like $\tilde{g}_{\omega l}^\Lambda$, also satisfy the wave equation (2.7), but with the significant difference that they are only defined in region I (see Fig. 1). To complement the definition of these functions we require the following initial conditions:

$$\tilde{f}_{\omega l}^{\text{in}} = \begin{cases} 0 & , \quad H_{\text{past}} \\ e^{-i\omega v} & , \quad \text{PNI} \end{cases} \quad , \quad \tilde{f}_{\omega l}^{\text{up}} = \begin{cases} e^{-i\omega u_{\text{ext}}} & , \quad H_{\text{past}} \\ 0 & , \quad \text{PNI} \end{cases} . \quad (2.12)$$

Due to the staticity of the background metric, the outer Eddington-Finkelstein modes $\tilde{f}_{\omega l}^{\text{in}}$ and $\tilde{f}_{\omega l}^{\text{up}}$ can be further decomposed into a time-dependent part and a radial function, satisfying an *ordinary* differential equation (ODE), which can be readily solved numerically. The decomposition is as follows:

$$\tilde{f}_{\omega l}^{\text{in}}(r, t) = e^{-i\omega t} \Psi_{\omega l}^{\text{in}}(r) \quad , \quad \tilde{f}_{\omega l}^{\text{up}}(r, t) = e^{-i\omega t} \Psi_{\omega l}^{\text{up}}(r). \quad (2.13)$$

Substituting these decompositions into Eq. (2.7) yields the following radial equation for $\Psi_{\omega l}^\Lambda$:

$$\Psi_{\omega l, r_* r_*}^\Lambda + [\omega^2 - V_l(r)] \Psi_{\omega l}^\Lambda = 0, \quad (2.14)$$

where the effective potential V_l is given by Eq. (2.8). In terms of the radial functions $\Psi_{\omega l}^\Lambda$, the initial conditions given in Eq. (2.12) are translated to

$$\Psi_{\omega l}^{\text{in}}(r) \cong \begin{cases} \tau_{\omega l}^{\text{in}} e^{-i\omega r_*} & , \quad r_* \rightarrow -\infty \\ e^{-i\omega r_*} + \rho_{\omega l}^{\text{in}} e^{i\omega r_*} & , \quad r_* \rightarrow \infty \end{cases} \quad (2.15)$$

and

$$\Psi_{\omega l}^{\text{up}}(r) \cong \begin{cases} e^{i\omega r_*} + \rho_{\omega l}^{\text{up}} e^{-i\omega r_*} & , \quad r_* \rightarrow -\infty \\ \tau_{\omega l}^{\text{up}} e^{i\omega r_*} & , \quad r_* \rightarrow \infty \end{cases} , \quad (2.16)$$

where $\rho_{\omega l}^\Lambda$ and $\tau_{\omega l}^\Lambda$ are the reflection and transmission coefficients (corresponding to the mode $\tilde{f}_{\omega l}^\Lambda$), respectively. Solving numerically Eq. (2.14) together with the boundary conditions (2.15) and (2.16) yields $\Psi_{\omega l}^\Lambda(r)$, which then gives the modes $f_{\omega lm}^{\text{in}}$ and $f_{\omega lm}^{\text{up}}$ using Eqs. (2.13) and (2.11).

We can now similarly define the two sets of *inner Eddington-Finkelstein modes*, which are again decomposed according to Eq. (2.11), and the corresponding functions $\tilde{f}_{\omega l}^\Lambda$ also satisfy Eq. (2.7). It is very analogous to the above definition of the *outer Eddington-Finkelstein modes*, except that here Λ denotes “right” (R) and “left” (L), corresponding to the following initial conditions on the left and right event horizons ²:

$$\tilde{f}_{\omega l}^{\text{L}} = \begin{cases} e^{-i\omega u_{\text{int}}} & , \quad H_L \\ 0 & , \quad H_R \end{cases} \quad , \quad \tilde{f}_{\omega l}^{\text{R}} = \begin{cases} 0 & , \quad H_L \\ e^{-i\omega v} & , \quad H_R \end{cases} . \quad (2.17)$$

Note that these modes are defined only in region II , depicted in Fig. 1.

² As was already stressed in [33], the “right” and “left” modes defined in the interior region of the BH are only introduced for mathematical convenience and are not used here for the definition of any quantum state.

Just like the outer Eddington-Finkelstein modes, the inner Eddington-Finkelstein modes $\tilde{f}_{\omega l}^L$ and $\tilde{f}_{\omega l}^R$ can be further decomposed into a t -dependent part and a radial function, satisfying the same radial equation (2.14) as the external radial function $\Psi_{\omega l}^\Lambda$ (with some, obviously different, appropriate initial conditions which will be specified below). Note however the important fact that upon crossing the event horizon from the exterior region to the interior, the roles of the t and r coordinates as timelike and spacelike, respectively, are reversed. As a result, outside the BH there is a single t -dependent part, namely $e^{-i\omega t}$, in the decomposition of both $\tilde{f}_{\omega l}^{\text{in}}$ and $\tilde{f}_{\omega l}^{\text{up}}$. However, inside the BH the decomposition of $\tilde{f}_{\omega l}^L$ and $\tilde{f}_{\omega l}^R$ is as follows:

$$\tilde{f}_{\omega l}^L(r, t) = e^{i\omega t} \psi_{\omega l}(r) \quad , \quad \tilde{f}_{\omega l}^R(r, t) = e^{-i\omega t} \psi_{\omega l}(r). \quad (2.18)$$

Notice that in (2.18) the two modes differ in their t -dependent part. At the same time, these two modes share a *single* radial function $\psi_{\omega l}(r)$ - unlike the external Eddington-Finkelstein modes which involve two different radial functions, $\Psi_{\omega l}^{\text{in}}(r)$ and $\Psi_{\omega l}^{\text{up}}(r)$. Substitution of the decompositions (2.18) into Eq. (2.7) yields the aforementioned radial equation for $\psi_{\omega l}$, namely

$$\psi_{\omega l, r_* r_*} + [\omega^2 - V_l(r)] \psi_{\omega l} = 0. \quad (2.19)$$

In terms of this radial function, the initial conditions given in Eq. (2.17) reduce to the single condition

$$\psi_{\omega l} \cong e^{-i\omega r_*}, \quad r_* \rightarrow -\infty. \quad (2.20)$$

Then, solving numerically the ODE (2.19) together with the initial condition (2.20) yields $\psi_{\omega l}(r)$. Using Eqs. (2.18), (2.11) and (2.6) will then give us the modes $f_{\omega l m}^L$ and $f_{\omega l m}^R$.

Finally, we are also interested in the Hartle-Hawking state [30, 31], denoted by $|0\rangle_H$. Unlike the Boulware state, the Hartle-Hawking state does not correspond to the conventional concept of a vacuum. The RSET is regular on the event horizons, both past (H_{past}) and future (H_R), but the state is not empty at infinity. In fact, it corresponds to a thermal bath of radiation at infinity. Although it is customary to define it using an analytic continuation to the Euclidean section, for our current purposes we are merely interested in the mode structure of this state; The Hartle-Hawking modes assume the form of Kruskal modes on both the past (H_{past}) and future (H_R) event horizons, more specifically, $e^{-i\omega U}$ at H_{past} and $e^{-i\omega V}$ at H_R .

C. The Unruh and Hartle-Hawking states Hadamard functions inside the black hole

Recall that the inner Eddington-Finkelstein modes can be expressed in terms of a single radial function, $\psi_{\omega l}(r)$ [see Eq. (2.18)] which can be computed numerically. We intend to use this fact, and we are thus in need for an expression of the Hadamard function, inside the BH, in terms of the inner Eddington-Finkelstein modes (in both states of interest, namely Unruh and Hartle-Hawking).

Recall that in Eq. (2.10) the scalar field operator was decomposed in terms of the Unruh modes. Substitution of this expression into the definition of the Hadamard function [see Eq. (1.3)], yields a mode-sum expression for the Hadamard function in terms of the Unruh modes. As the latter are continuously defined throughout both regions *I* and *II* of Fig. 1 (as discussed in Sec. IIB), this expression applies to both the exterior and interior regions of the BH spacetime. As is thoroughly elaborated in [33], in both the exterior and interior regions, these Unruh modes can be re-expressed in terms of the outer and inner Eddington-Finkelstein modes. Using these relations, expressions for the Unruh state two-point function outside and inside the BH, in terms of the outer and inner Eddington-Finkelstein modes, may be obtained.

This procedure was carried out in [34] for the Feynman propagator outside the event horizon of Schwarzschild spacetime. When this procedure is implemented to the Hadamard Green function it yields

$$G_U^{(1)}(x, x') = \int_0^\infty d\omega \sum_{l, m} \left[\coth\left(\frac{\pi\omega}{\kappa}\right) \{f_{\omega l m}^{\text{up}}(x), f_{\omega l m}^{\text{up}*}(x')\} + \{f_{\omega l m}^{\text{in}}(x), f_{\omega l m}^{\text{in}*}(x')\} \right], \quad (2.21)$$

where the subscript U stands for ‘‘Unruh state’’, and the curly brackets denote symmetrization with respect to the arguments x and x' , i.e.

$$\{A(x), B(x')\} = A(x)B(x') + A(x')B(x).$$

A similar procedure can be applied to the Hartle-Hawking Hadamard function, yielding [34]:

$$G_H^{(1)}(x, x') = \int_0^\infty d\omega \sum_{l,m} \coth\left(\frac{\pi\omega}{\kappa}\right) [\{f_{\omega lm}^{\text{up}}(x), f_{\omega lm}^{\text{up}*}(x')\} + \{f_{\omega lm}^{\text{in}}(x), f_{\omega lm}^{\text{in}*}(x')\}], \quad (2.22)$$

where the subscript H stands for ‘‘Hartle-Hawking state’’. This expression may actually be obtained by replacing the above Unruh modes with corresponding modes associated with the Hartle-Hawking state, which assume the form of Kruskal modes at both the past and future horizons³.

However, for the purpose of the present work we are interested in the expressions for the Unruh state and Hartle-Hawking state Hadamard functions *inside* the BH. These were obtained in [33] and we merely quote here the final results, which we express here in the following schematic form:

$$G_U^{(1)}(x, x') = \int_0^\infty d\omega \sum_{l,m} \tilde{E}_{\omega lm}^U(x, x')$$

and

$$G_H^{(1)}(x, x') = \int_0^\infty d\omega \sum_{l,m} \tilde{E}_{\omega lm}^H(x, x'),$$

where

$$\begin{aligned} \tilde{E}_{\omega lm}^U(x, x') &= \coth\left(\frac{\pi\omega}{\kappa}\right) \{f_{\omega lm}^L(x), f_{\omega lm}^{L*}(x')\} + \left[\coth\left(\frac{\pi\omega}{\kappa}\right) |\rho_{\omega l}^{\text{up}}|^2 + |\tau_{\omega l}^{\text{up}}|^2 \right] \{f_{\omega lm}^R(x), f_{\omega lm}^{R*}(x')\} \\ &\quad + 2\text{csch}\left(\frac{\pi\omega}{\kappa}\right) \text{Re} \left[\rho_{\omega l}^{\text{up}} \left\{ f_{\omega lm}^R(x), f_{(-\omega)lm}^{L*}(x') \right\} \right], \end{aligned} \quad (2.23)$$

and

$$\begin{aligned} \tilde{E}_{\omega lm}^H(x, x') &= \coth\left(\frac{\pi\omega}{\kappa}\right) [\{f_{\omega lm}^L(x), f_{\omega lm}^{L*}(x')\} + \{f_{\omega lm}^R(x), f_{\omega lm}^{R*}(x')\}] \\ &\quad + 2\text{csch}\left(\frac{\pi\omega}{\kappa}\right) \text{Re} \left[\rho_{\omega l}^{\text{up}} \left\{ f_{\omega lm}^R(x), f_{(-\omega)lm}^{L*}(x') \right\} \right]. \end{aligned} \quad (2.24)$$

As already mentioned, the inner Eddington-Finkelstein modes can be computed [via Eqs. (2.18) and (2.11)] by numerically solving the ODE (2.19) for $\psi_{\omega l}$ in the interior region together with the initial condition given by Eq. (2.20). This concludes the numerical computation of the Unruh and Hartle-Hawking states Hadamard functions in the BH interior.

III. ANGULAR-SPLITTING VARIANT OF THE PMR METHOD: THE PRACTICAL RECIPE

Recall that the task at hand is to compute the renormalized $\langle \hat{\Phi}^2 \rangle$ in the Schwarzschild BH interior. As mentioned in the introduction, a frequently employed technique to regularize $\langle \hat{\Phi}^2(x) \rangle$ is point splitting. This method may be recast in the form

$$\langle \Phi^2(x) \rangle_{ren} = \lim_{x' \rightarrow x} \left[\langle \hat{\Phi}(x) \hat{\Phi}(x') \rangle - G_{DS}(x, x') \right]. \quad (3.1)$$

For our purposes it will be convenient to rewrite Eq. (3.1) in terms of the Hadamard function, as follows:

$$\langle \Phi^2(x) \rangle_{ren} = \lim_{x' \rightarrow x} \left[\frac{1}{2} G^{(1)}(x, x') - G_{DS}(x, x') \right]. \quad (3.2)$$

³ More technically, this may be achieved by changing $e^{-i\omega v} \rightarrow e^{-i\omega V}$ at PNI in Eq. (2.9).

In the last two equations, $G_{DS}(x, x')$ is the DeWitt-Schwinger counterterm, which in our case, that is for a massless scalar field propagating in a Schwarzschild background spacetime, takes the form⁴ [15, 22]

$$G_{DS}(x, x') = \frac{1}{8\pi^2\sigma}. \quad (3.3)$$

Here σ is the biscalar of geodesic separation, equal to one half the square of the distance between the points x and x' along the shortest geodesic connecting them. A key feature of the DeWitt-Schwinger counterterm is that it is a purely local geometric object, independent of the quantum state, and it fully embodies the singular part of the Hadamard function at the coincidence limit.

As we already mentioned in the introduction, the field's modes are usually not known analytically, and in particular in BH background spacetimes, the modes can only be numerically computed. In such cases, the direct evaluation of the coincidence limit of the splitted expression in Eq. (3.2) becomes impractical, especially because it requires increasingly high numerical accuracy when x' approaches x . This obstacle is overcome by the PMR method. We will not be reviewing the construction of the PMR method here. For a detailed exposition of the method, see [24, 25]. In what follows we merely present the key steps involved in the implementation of the angular-splitting variant [25] of the method.

In Eqs. (2.23) and (2.24) we expressed the Hadamard functions in Unruh and Hartle-Hawking states, respectively, in terms of the inner Eddington-Finkelstein modes, which will be our modes of interest in what follows. Recall from Eqs. (2.11) and (2.18) that the field modes can be decomposed as follows:

$$f_{\omega lm}^L(x) = e^{i\omega t} Y_{lm}(\theta, \varphi) \bar{\psi}_{\omega l}(r), \quad f_{\omega lm}^R(x) = e^{-i\omega t} Y_{lm}(\theta, \varphi) \bar{\psi}_{\omega l}(r). \quad (3.4)$$

where we introduced the notation

$$\bar{\psi}_{\omega l}(r) = (4\pi |\omega|)^{-1/2} \frac{1}{r} \psi_{\omega l}(r). \quad (3.5)$$

The functions $\psi_{\omega l}$ satisfy the ODE (2.19), along with the initial condition given by Eq. (2.20).

The final outcome of the PMR method is entirely expressed in terms of the coincidence limit $x' \rightarrow x$ of the quantities $\tilde{E}_{\omega lm}^U$ and $\tilde{E}_{\omega lm}^H$ defined in Eqs. (2.23) and (2.24) respectively. We therefore define the coincidence limit of these two quantities (multiplied by $2\pi/(2l+1)$ for later convenience):

$$E_{\omega l}^U(r) = \sum_m \frac{2\pi}{2l+1} \tilde{E}_{\omega lm}^U(x, x'=x), \quad E_{\omega l}^H(r) = \sum_m \frac{2\pi}{2l+1} \tilde{E}_{\omega lm}^H(x, x'=x) \quad (3.6)$$

Note that the dependence on θ , φ and t cancels out upon taking the coincidence limit and summing over m . It is convenient to express $E_{\omega l}^U(r)$ and $E_{\omega l}^H(r)$ directly in terms of the radial function $\psi_{\omega l}$ [rather than the functions $f_{\omega lm}^\Lambda$ appearing in Eqs. (2.23) and (2.24)], since this is the function we actually obtain by solving numerically the radial equation (2.19). To this end we recall that Eqs. (3.4) and (3.5) provide the relation between the functions $f_{\omega lm}^\Lambda$ and $\psi_{\omega l}$, and further note that $\psi_{(-\omega)l} = \psi_{\omega l}^*$. It thus readily follows that

$$E_{\omega l}^U(r) = \left[\coth\left(\frac{\pi\omega}{\kappa}\right) \left(|\rho_{\omega l}^{\text{up}}|^2 + 1 \right) + |\tau_{\omega l}^{\text{up}}|^2 \right] |\bar{\psi}_{\omega l}|^2 + 2\text{csch}\left(\frac{\pi\omega}{\kappa}\right) \text{Re}(\rho_{\omega l}^{\text{up}} \bar{\psi}_{\omega l}^2) \quad (3.7)$$

and

$$E_{\omega l}^H(r) = 2 \left[\coth\left(\frac{\pi\omega}{\kappa}\right) |\bar{\psi}_{\omega l}|^2 + \text{csch}\left(\frac{\pi\omega}{\kappa}\right) \text{Re}(\rho_{\omega l}^{\text{up}} \bar{\psi}_{\omega l}^2) \right], \quad (3.8)$$

where we again used Eq. (3.5) to translate these expressions from $\psi_{\omega l}$ to $\bar{\psi}_{\omega l}$ for compactness.

For convenience, in what follows unless specifically stated otherwise, we shall denote both $E_{\omega l}^U$ and $E_{\omega l}^H$ as $E_{\omega l}$ because the next stages treat them in exactly the same way. Following the PMR prescription, we define the following integral

$$F(l, r) \equiv \int_0^\infty d\omega [E_{\omega l}(r) - E_{\omega, l=0}(r)]. \quad (3.9)$$

⁴ This expression for the DeWitt-Schwinger counterterm actually applies to a massless scalar field propagating in any vacuum background spacetime.

We further define

$$F_{sing}(l, r) = -8\pi a(r) h(l), \quad (3.10)$$

which captures the singular piece of the function $F(l, r)$. Here, the function $h(l)$ is the *Harmonic Number* defined by

$$h(l) \equiv \sum_{k=1}^l \frac{1}{k}, \quad h(0) \equiv 0,$$

and $a(r)$ is a coefficient appearing in the expansion of G_{DS} in powers of $\sin(\varepsilon/2)$ (where ε is the splitting in θ), a procedure thoroughly explained in [25]. Another such coefficient that will be of use later is $d(r)$. These coefficients generally depend on the mass of the field, on its coupling constant ξ , and on the background metric. For a massless scalar field and a Schwarzschild background geometry they assume the simple forms

$$a(r) = \frac{1}{16\pi^2 r^2}, \quad d(r) = -\frac{M}{24\pi^2 r^3}. \quad (3.11)$$

Therefore we have

$$F_{sing}(l, r) = -\frac{1}{2\pi r^2} h(l). \quad (3.12)$$

Notice that, just like h , F_{sing} diverges logarithmically with l .

We now remove the singular piece from the function F by subtracting F_{sing} from it, thereby obtaining a new regularized function denoted by F_{reg} , that is

$$F_{reg}(l, r) \equiv F(l, r) - F_{sing}(l, r). \quad (3.13)$$

It turns out that subtracting F_{sing} is generally insufficient for the convergence of the sum over l , and that in fact, $F_{reg}(l, r)$ converges to a non-zero constant limit as $l \rightarrow \infty$, hence the naive sum over l of this quantity [multiplied by $2l + 1$, as a compensation for the denominators introduced in Eq. (3.6)] would diverge. This divergence reflects the fact that the counterterm provides only partial information about the mode-sum singularity, as information is lost in the Legendre decomposition. This obstacle is referred to as the *blind spots* phenomenon in Ref. [25], and to circumvent it, a process called *self-cancellation* is employed. The idea is that the non-zero limiting value of $F_{reg}(l, r)$ ought to be further subtracted for the sum over l to converge, and our technical means of achieving it is by defining the following sequence of partial sums⁵

$$H(l, r) \equiv \sum_{k=0}^l \frac{2k+1}{4\pi} [F_{reg}(k, r) - F_{reg}(l, r)]. \quad (3.14)$$

The final expression for $\langle \Phi^2 \rangle_{ren}$ is

$$\langle \Phi^2(x) \rangle_{ren} = \hbar \left[\lim_{l \rightarrow \infty} H(l, r) - d(r) \right]. \quad (3.15)$$

Recall that H is constructed from functions originating in $E_{\omega l}$. In order to obtain the Unruh state $\langle \Phi^2 \rangle_{ren}$ from (3.15), one has to construct H from $E_{\omega l}^U$ of Eq. (3.7). Similarly, obtaining the Hartle-Hawking state $\langle \Phi^2 \rangle_{ren}$ requires the use of $E_{\omega l}^H$ defined in (3.8).

Let us summarize. The final expression for the renormalized expectation value of $\hat{\Phi}^2$ is given in (3.15), with H defined in (3.14). There we used the function F_{reg} which is specified in (3.13). This function involves the quantity F_{sing} defined for our specific case in (3.12). It further requires the use of F defined in (3.9), which in turn is constructed from $E_{\omega l}$. As we mentioned above, the latter quantity is denoted by $E_{\omega l}^U$ in Unruh state [see (3.7)] and by $E_{\omega l}^H$ in Hartle-Hawking state [see (3.8)]. These are computed from the radial functions, $\bar{\psi}_{\omega l}$, defined in Eq. (3.5) in terms of $\psi_{\omega l}$. The latter is obtained by numerically solving the radial equation (2.19) with the initial conditions (2.20).

⁵ Note that the limit $H(l \rightarrow \infty, r)$ is equivalent to the sum over l of the sequence $\frac{2l+1}{4\pi} [F_{reg}(l, r) - F_{reg}(l \rightarrow \infty, r)]$.

IV. NUMERICAL IMPLEMENTATION: $\langle \Phi^2 \rangle_{ren}$ INSIDE A SCHWARZSCHILD BLACK HOLE

Our final expression for $\langle \Phi^2 \rangle_{ren}$ was constructed in Sec. III using the integrands (3.7) and (3.8). These integrands consist of the radial function $\psi_{\omega l}$ and also the reflection coefficient $\rho_{\omega l}^{up}$ and the transmission coefficient $\tau_{\omega l}^{up}$. The computation of $\langle \hat{\Phi}^2(x) \rangle_{ren}$ therefore requires the numerical computation of the three quantities $\bar{\psi}_{\omega l}(r)$, $\rho_{\omega l}^{up}$ and $\tau_{\omega l}^{up}$.

The radial equation (2.19) together with the initial condition (2.20) was solved numerically for $\psi_{\omega l}$ using the ODE solver embedded in Mathematica. It was solved for 11 l values ($0 \leq l \leq 10$), for each l in the range $\omega \in [0, 20]$, with a uniform spacing $d\omega = 10^{-2}$. Then $\bar{\psi}_{\omega l}$ was constructed from $\psi_{\omega l}$ using Eq. (3.5).

The transmission ($\tau_{\omega l}^{up}$) and reflection ($\rho_{\omega l}^{up}$) coefficients for each ωl mode were extracted from the numerical solution of Eq. (2.14) for the radial function $\Psi_{\omega l}$ outside the BH. Boundary conditions were specified at the past horizon, where the radial functions assumed the form $\Psi_{\omega l} = e^{-i\omega r^*}$, and the solution was evolved towards $r \rightarrow \infty$. Here, as well, the calculation was carried out by the ODE solver embedded in Mathematica, for the same modes of l and ω as described above.

In order to illustrate the various stages of the renormalization procedure, let us follow an example of the computation of $\langle \Phi^2 \rangle_{ren}$ for $r = 1.4M$ in the Hartle-Hawking state. Figure 2a displays $E_{\omega l}^H$ as a function of ω for $l = 1$. Here and

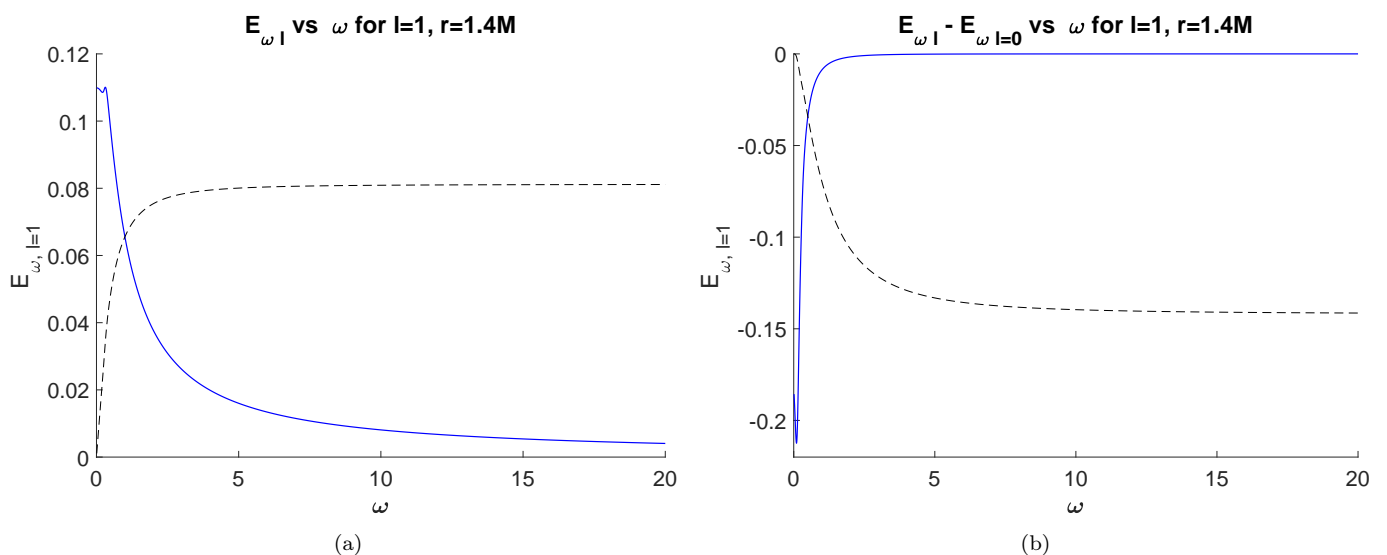


Figure 2: (a) Blue curve: the numerically computed $E_{\omega, l=1}^H$, as defined in (3.8), evaluated at $r = 1.4M$. The dashed black curve is $\omega E_{\omega, l=1}^H$, indicating that the asymptotic behavior of $E_{\omega, l=1}^H$ at large ω is proportional to ω^{-1} . (b) Blue curve: the numerically computed difference $E_{\omega, l=1}^H - E_{\omega, l=0}^H$, evaluated at $r = 1.4M$. The dashed black curve is

$$8\omega^3 \left(E_{\omega, l=1}^H - E_{\omega, l=0}^H \right),$$

thus the asymptotic behavior of the difference at large ω is proportional to ω^{-3} .

in all the graphs below we use units where $M = 1$ and $G = c = 1$. As is indicated by the dashed black curve, $E_{\omega l}^H$ behaves asymptotically at large ω as $1/\omega$, therefore its integral diverges at infinity. This divergence is regularized by subtracting from the integrand the $l = 0$ mode, i.e. $E_{\omega, l=0}^H$, as was done in Eq. (3.9). This regularization results in an integrand which behaves asymptotically as $1/\omega^3$, as indicated by the dashed black curve in Fig. 2b, leading to a convergent integral.

Even after the aforementioned regularization of the integral over ω , the convergence is still rather slow, and the integration requires a very large range of ω in order to achieve a result with sufficient accuracy. We circumvented this difficulty by employing a large- ω expansion⁶ of $|\psi_{\omega l}(r)|^2$ up to order ω^{-13} in the integral from $\omega = 20$ to infinity.

Recall from (3.9) that the integral over ω gives $F(l, r)$, displayed in Fig. 3a as a series of blue dots. Note the logarithmic behavior at large values of l , which importantly, characterizes $F_{sing}(l, r)$ as well [also shown in Fig. 3a in red]. Of course, the sum over l of $(2l + 1)F(l, r)$ then diverges, demonstrating the need for a subtraction of the

⁶ We followed here the large- ω expansion procedure presented in Appendix D in [25].

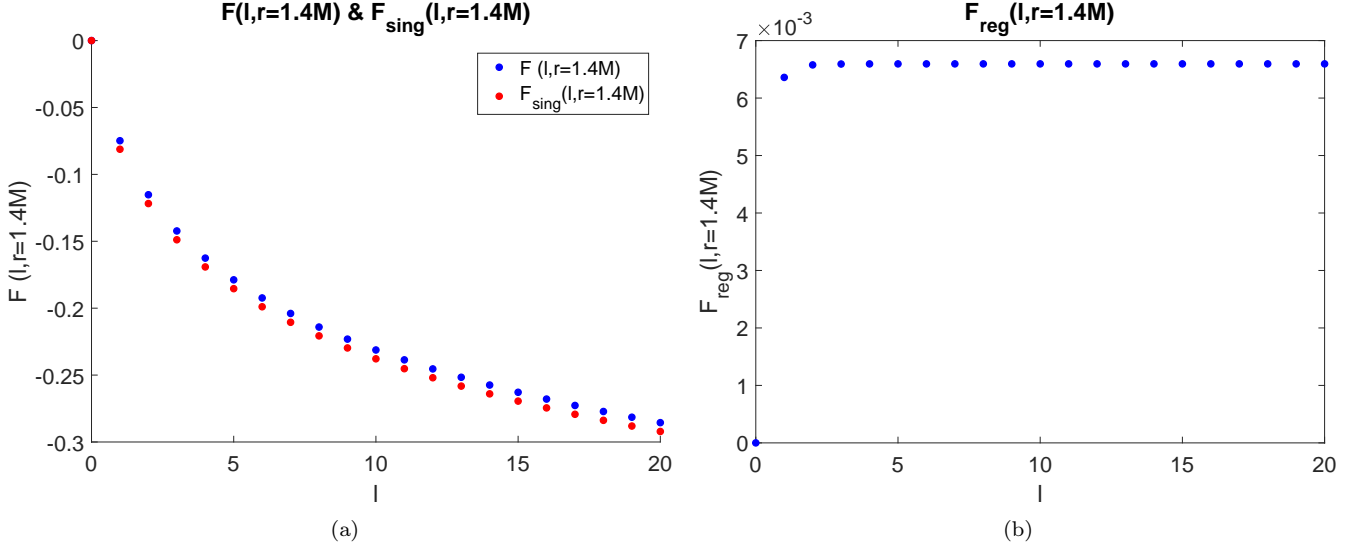


Figure 3: (a) The numerically computed $F(l, r = 1.4M)$, as defined in (3.9), represented by blue dots. The analytically computed function $F_{sing}(l, r = 1.4M)$, as defined in (3.12), appears in red dots. (b) $F_{reg}(l, r = 1.4M)$ as defined in (3.13), i.e. the difference between the two curves in Fig. 3a. It quickly converges to a constant (the so-called “blind-spot” mentioned in Sec. III), which will require self-cancellation.

divergent piece. This is predominantly achieved in Eq. (3.13) by subtracting $F_{sing}(l, r)$, resulting in $F_{reg}(l, r)$ which behaves as a constant at large values of l (see Fig. 3b).

We next self-cancel the “blind spot” by constructing the sequence $H(l, r)$ according to Eq. (3.14). This quantity is presented in Fig. 4a. Note the rapid convergence of $H(l, r)$, most clearly seen in the zoom displayed in Fig. 4b.

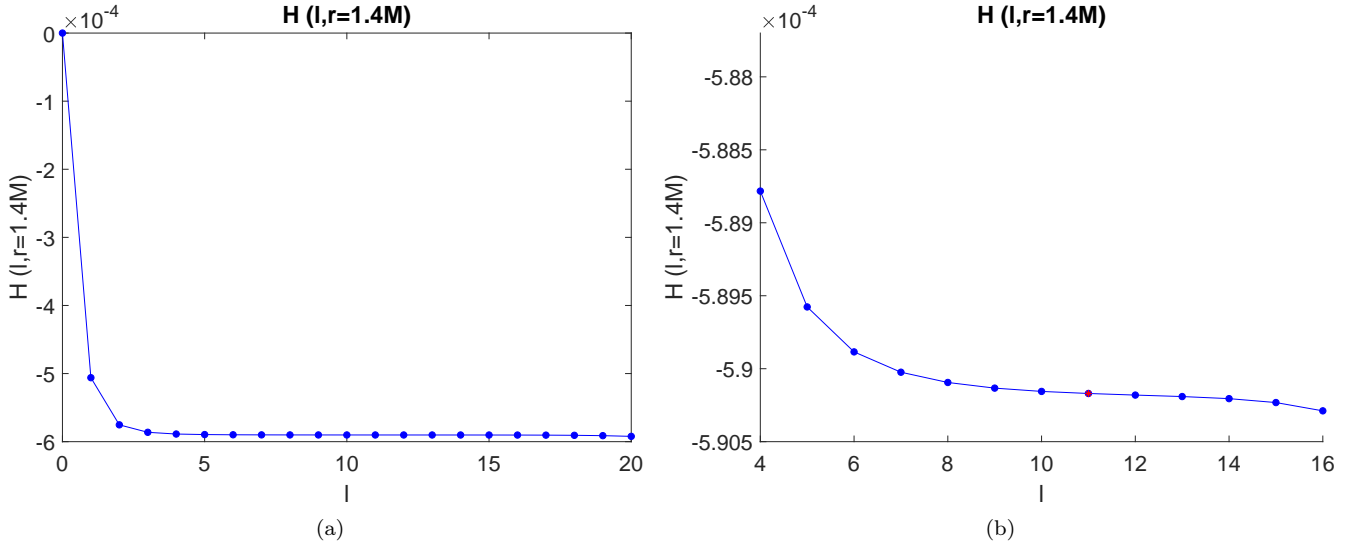


Figure 4: (a) The numerically computed sequence $H(l, r = 1.4M)$, constructed according to Eq. (3.14). It clearly rapidly converges at large l . (b) A closer look at the plateau region in Fig. 4a. In this scale, the growth of a numerical error at large l is apparent. The red dot indicates the estimated optimal l value for the numerical evaluation of the large- l limit of H . This l is automatically selected by an algorithm that locates the value of l beyond which the numerical error begins to increase.

Finally, the large- l limit of $H(l, r)$ is taken, yielding the limiting value $-0.0005902 M^{-2}$. When substituted in Eq.

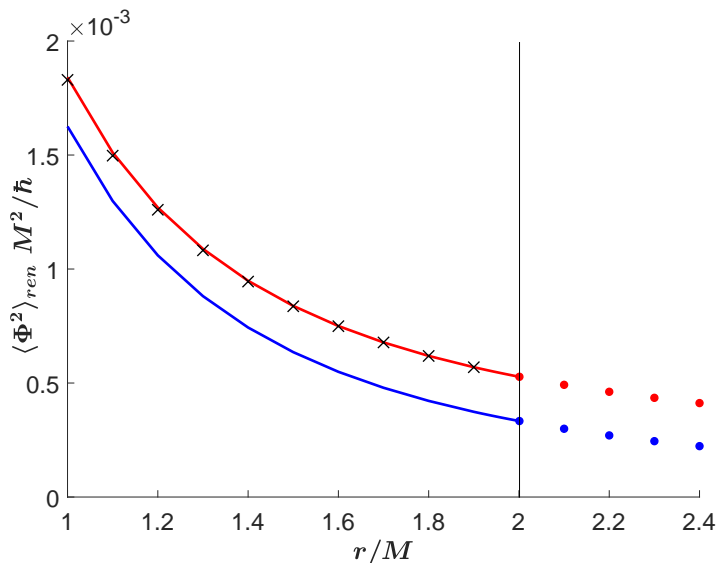


Figure 5: The solid red and blue lines represent our results for $\langle \hat{\Phi}^2(r) \rangle_{ren}$ in Hartle-Hawking state and in Unruh state, respectively, inside the BH. The red and blue dots represent the analogous results previously obtained outside the event horizon [25]. The event horizon is marked by the vertical black solid line. The results by Candela & Jensen for the Hartle-Hawking state appear as black “x” markers. Our results seem to agree at the event horizon with those of [25], and are in a fairly good agreement with those obtained by Candela & Jensen.

(3.15), it yields $\langle \hat{\Phi}^2(r = 1.4M) \rangle_{ren} \cong 0.0009484 \hbar M^{-2}$ in Hartle-Hawking state.

In the same way, we computed $\langle \hat{\Phi}^2(r) \rangle_{ren}$ for different values of r in the domain⁷ $1 \leq r \leq 1.99999$. The same computation scheme was then applied to the Unruh state as well. The results are presented in Fig. 5 which displays $\langle \hat{\Phi}^2 \rangle_{ren}$ in both Hartle-Hawking and Unruh states for various values of r , together with corresponding results previously obtained outside the BH [25]. We estimate that the numerical error is typically around two parts in 10^3 or smaller. Our results for Hartle-Hawking state are compared to previous results published by Candela and Jensen [29] (black crosses), showing a fairly good agreement⁸.

Fig. 6 displays $\langle \hat{\Phi}^2(r) \rangle_{ren}$ for different values of r in the vicinity of the event horizon, showing results for both the interior and the exterior regions. Extrapolation of the results, from both inside and outside the BH, to the event horizon shows good agreement, with a difference of about 0.03% (fully consistent with our estimated numerical errors). It further shows a difference of only $\sim 0.02\%$ from the analytical result Candela obtained [34] for the Hartle-Hawking state $\langle \hat{\Phi}^2 \rangle_{ren}$ at the event horizon, which equals to $1/192\pi^2 M^2 \simeq 0.0005277 M^{-2}$.

V. DISCUSSION

In this work we considered a massless scalar field, and numerically computed $\langle \hat{\Phi}^2 \rangle_{ren}$ inside a Schwarzschild BH, in both Hartle-Hawking and Unruh quantum states. We performed the computation by employing a recently developed numerical implementation method of the point-splitting renormalization scheme [24, 25], which we referred to as the “PMR” method. This method has been previously utilized to numerically compute $\langle \hat{\Phi}^2 \rangle_{ren}$ and $\langle \hat{T}_{\mu\nu} \rangle_{ren}$ outside Schwarzschild, RN (unpublished) and Kerr BHs [24–28]. Here we report the first application of the PMR method in BH interiors, as part of an ongoing program to compute the RSET inside BHs and, particularly, explore how it modifies the geometrical structure of the inner (Cauchy) horizon of RN and Kerr BHs.

In order to facilitate the computation of $\langle \hat{\Phi}^2 \rangle_{ren}$, we used the results of Ref. [33] to express the Hartle-Hawking and Unruh states Hadamard functions in the interior of a Schwarzschild BH in terms of a sum of what we call *inner Eddington-Finkelstein modes*. These modes can be decomposed into radial functions satisfying an ODE, which we

⁷ We stopped our computation at $r = 1$, since the numerical difficulties grow significantly as r decreases.

⁸ With a difference of less than 1% (which probably results from numerical inaccuracy), improving markedly to less than 0.1% in the region $1.6 \leq r \leq 1.9$.

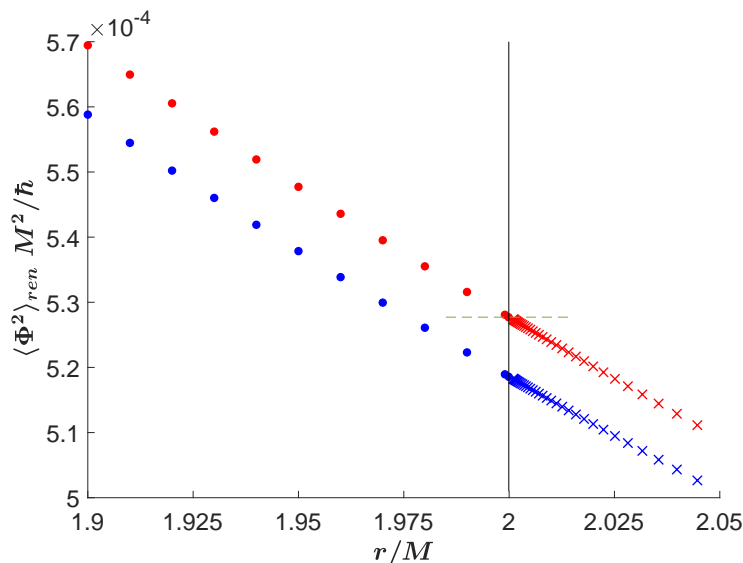


Figure 6: Near-horizon results for $\langle \Phi^2(r) \rangle_{ren}$ calculated for different values of r . The red and blue dots represent the results for $\langle \Phi^2 \rangle_{ren}$ in Hartle-Hawking state and in Unruh state, respectively, inside the BH. Note that the results for the Unruh state (blue) were shifted here by an amount $+0.000185$ for convenience of display. [This shift allows us to present the two sets of data (Unruh and Hartle-Hawking) on the same graph, with sufficient resolution at the vertical scale.] The red and blue “x” markers represent the analogous results previously obtained outside the event horizon, using the method described in [25]. The two sets of results (external and internal ones) nicely agree at the event horizon (vertical black solid line). They also show good agreement with the analytical result obtained by Candelas at the event horizon (in the Hartle-Hawking state), marked here by the short green horizontal dashed line.

solve numerically. We subsequently employed the angular-splitting variant [25] of the PMR method, and obtained $\langle \Phi^2 \rangle_{ren}$ for Hartle-Hawking and Unruh states inside a Schwarzschild BH.

Our results for the Hartle-Hawking state were compared with previous results by Candelas and Jensen [29] with a fairly good agreement, as seen in Fig. 5. The results we obtained for both Hartle-Hawking and Unruh states further agree at the event horizon with previous results for $\langle \Phi^2 \rangle_{ren}$ obtained outside the BH in Ref. [25]. Our results for Hartle-Hawking state at the event horizon also agree with previous analytical results obtained by Candelas [34].

We are generally interested in the internal structure of BHs and, in particular, in the influence of quantum fluxes on the BH interior geometry. Understanding this issue ultimately requires the investigation of the behavior of $\langle \hat{T}_{\mu\nu} \rangle_{ren}$ in the interior of BHs. As a first stage towards this goal, we set out to compute $\langle \Phi^2 \rangle_{ren}$ in BH interiors, starting with the case of a Schwarzschild BH as elaborated in the present paper. It would be interesting, and important in the context of the aforementioned research program, to further extend the present work and compute $\langle \Phi^2 \rangle_{ren}$ inside RN [36] and Kerr BHs. Since the latter are in fact the real astrophysical BHs, it would be of special interest to extend this work to Kerr BHs in the future. To accomplish that, one would have to resort to the t -splitting variant (or perhaps φ -splitting variant) of the PMR method, because the angular-splitting variant will not work in the Kerr case. Employing the t -splitting variant will have the additional benefit of providing independent results which would serve to corroborate those presented here for the interior of Schwarzschild BHs, obtained using the angular-splitting variant.

In the next stage, it will be necessary to extend the present analysis of quantum effects in BH interiors from $\langle \Phi^2 \rangle_{ren}$ to the RSET. Especially in BHs with inner horizons, and most importantly inside Kerr BHs.

Beyond the challenging task of computing $\langle \hat{T}_{\mu\nu} \rangle_{ren}$ throughout the interior of BHs, in order to achieve a more complete understanding of semiclassical BH interiors, we shall have to confront the much harder challenge of self-consistently analyzing the back-reaction effect of these quantum fluxes on the internal geometry (via the semiclassical Einstein equation). Although, at the moment this goal is far out of reach.

In addition, it would be particularly interesting to consider the fluxes due to the quantum electromagnetic field (and perhaps also due to quantized gravitational perturbations?). These are the more realistic physical fields, and we hope their effects will be studied in the future.

Acknowledgments

This research was supported by the Asher Fund for Space Research at the Technion.

-
- [1] A. Ori, *Structure of the singularity inside a realistic rotating black hole*, Phys. Rev. Lett. **68**, 2117 (1992).
- [2] P. R. Brady, S. Droz, and S. M. Morsink, *Late-time singularity inside nonspherical black holes*, Phys. Rev. D **58**, 084034 (1998).
- [3] A. Ori, *Oscillatory null singularity inside realistic spinning black holes*, Phys. Rev. Lett. **83**, 5423 (1999).
- [4] A. Ori, *Evolution of linear gravitational and electromagnetic perturbations inside a kerr black hole*, Phys. Rev. D **61**, 024001 (1999).
- [5] M. Dafermos and J. Luk, *The interior of dynamical vacuum black holes I: The C^0 -stability of the Kerr Cauchy horizon*, (2017), arXiv:1710.01722 [gr-qc].
- [6] W. A. Hiscock, *Evolution of the interior of a charged black hole*, Phys. Lett. A **83**, 110 (1981).
- [7] E. Poisson and W. Israel, *Internal structure of black holes*, Phys. Rev. D **41**, 1796 (1990).
- [8] A. Ori, *Inner structure of a charged black hole: An exact mass-inflation solution*, Phys. Rev. Lett. **67**, 789 (1991).
- [9] P. R. Brady and J. D. Smith, *Black hole singularities: a numerical approach*, Phys. Rev. Lett. **75**, 1256 (1995).
- [10] L. M. Burko, *Structure of the black hole's cauchy-horizon singularity*, Phys. Rev. Lett. **79**, 4958 (1997).
- [11] D. Marolf and A. Ori, *Outgoing gravitational shock wave at the inner horizon: The late-time limit of black hole interiors*, Phys. Rev. D **86**, 124026 (2012).
- [12] E. Eilon and A. Ori, *Numerical study of the gravitational shock wave inside a spherical charged black hole*, Phys. Rev. D **94**, 104060 (2016).
- [13] E. Eilon, *Gravitational shock wave inside a steadily-accreting spherical charged black hole*, Phys. Rev. D **95**, 044041 (2017).
- [14] S. W. Hawking, *Particle creation by black holes*, Commun. Math. Phys. **43**, 199 (1975).
- [15] S. M. Christensen, *Vacuum expectation value of the stress tensor in an arbitrary curved background: The covariant point-separation method*, Phys. Rev. D **14**, 2490 (1976).
- [16] S. M. Christensen, *Regularization, renormalization, and covariant geodesic point separation*, Phys. Rev. D **17**, 946 (1978). P. Candelas and K. W. Howard, *Vacuum $\langle\phi^2\rangle$ in Schwarzschild spacetime*, Phys. Rev. D **29**, 1618 (1984).
- [17] B. S. DeWitt, *Dynamical Theory of Groups and Fields* (Gordon and Breach, New York, 1965).
- [18] J. Schwinger, *On Gauge Invariance and Vacuum Polarization*, Phys. Rev. **82**, 664 (1951).
- [19] N. D. Birrell and P. C. W. Davies, *Quantum fields in curved space* (Cambridge: Cambridge University Press, 1982).
- [20] K. W. Howard, *Vacuum $\langle T_{\mu}^{\nu}\rangle$ in Schwarzschild spacetime*, Phys. Rev. D **30**, 2532 (1984).
- [21] P. R. Anderson, *A method to compute $\langle\phi^2\rangle$ in asymptotically flat, static, spherically symmetric spacetimes*, Phys. Rev. D **41**, 1152 (1990).
- [22] P. R. Anderson, W. A. Hiscock, and D. A. Samuel, *Stress-energy tensor of quantized scalar fields in static spherically symmetric spacetimes*, Phys. Rev. D **51**, 4337 (1995).
- [23] P. Taylor and C. Breen, *Mode-sum prescription for vacuum polarization in black hole spacetimes in even dimensions*, Phys. Rev. D **96**, 105020 (2017).
- [24] A. Levi and A. Ori, *Pragmatic mode-sum regularization method for semiclassical black-hole spacetimes*, Phys. Rev. D **91**, 104028 (2015).
- [25] A. Levi and A. Ori, *Mode-sum regularization of $\langle\phi^2\rangle$ in the angular-splitting method*, Phys. Rev. D **94**, 044054 (2016).
- [26] A. Levi and A. Ori, *Versatile method for renormalized stress-energy computation in black-hole spacetimes*, Phys. Rev. Lett. **117**, 231101 (2016).
- [27] A. Levi, E. Eilon, A. Ori, and M. van de Meent, *Renormalized stress-energy tensor of an evaporating spinning black hole*, Phys. Rev. Lett. **118**, 141102 (2017).
- [28] A. Levi, *Renormalized stress-energy tensor for stationary black holes*, Phys. Rev. D **95**, 025007 (2017).
- [29] P. Candelas and B. P. Jensen, *Feynman Green function inside a Schwarzschild black hole*, Phys. Rev. D **33**, 1596 (1986).
- [30] J. B. Hartle and S. W. Hawking, *Path-integral derivation of black-hole radiance*, Phys. Rev. D **13**, 2188 (1976).
- [31] W. Israel, *Thermo-field dynamics of black holes*, Phys. Lett. A **57**, 107 (1976).
- [32] W. G. Unruh, *Notes on black-hole evaporation*, Phys. Rev. D **14**, 870 (1976).
- [33] A. Lanir, A. Levi, A. Ori, and O. Sela, *Two-point function of a quantum scalar field in the interior region of a Reissner-Nordström black hole*, Phys. Rev. D **97**, 024033 (2018).
- [34] P. Candelas, *Vacuum polarization in Schwarzschild spacetime*, Phys. Rev. D **21**, 2185 (1980).
- [35] D. G. Boulware, *Quantum field theory in Schwarzschild and Rindler spaces*, Phys. Rev. D **11**, 1404 (1975).
- [36] For a recent analytical work which provides a bound for the rate of divergence of $\langle\hat{\Phi}^2(x)\rangle_{ren}$ and $\langle\hat{T}_{\mu\nu}\rangle_{ren}$ inside RN BHs see O. Sela, *Quantum effects near the Cauchy horizon of a Reissner-Nordström black hole*, Phys. Rev. D **98**, 024025 (2018).